Critical endline of the finite temperature phase transition for $2+1$ flavor QCD around the SU(3)-flavor symmetric point

Yoshinobu Kuramashi,[1,2,3] Yoshifumi Nakamura,[3,4,*] Shinji Takeda,[5,3,†] and Akira Ukawa[3]

[1]*Faculty of Pure and Applied Sciences, University of Tsukuba, Tsukuba, Ibaraki 305-8571, Japan*
[2]*Center for Computational Sciences, University of Tsukuba, Tsukuba, Ibaraki 305-8577, Japan*
[3]*RIKEN Advanced Institute for Computational Science, Kobe, Hyogo 650-0047, Japan*
[4]*Graduate School of System Informatics, Department of Computational Sciences, Kobe University, Kobe, Hyogo 657-8501, Japan*
[5]*Institute of Physics, Kanazawa University, Kanazawa 920-1192, Japan*

(Received 16 May 2016; published 9 December 2016)

We investigate the critical endline of the finite temperature phase transition of QCD around the SU(3)-flavor symmetric point at zero chemical potential. We employ the renormalization-group improved Iwasaki gauge action and nonperturbatively $O(a)$-improved Wilson-clover fermion action. The critical endline is determined by using the intersection point of kurtosis, employing the multiparameter, multiensemble reweighting method to calculate observables off the SU(3)-symmetric point, at the temporal size $N_{\mathrm{T}}=6$ and lattice spacing as low as $a\approx 0.19$ fm. We confirm that the slope of the critical endline takes the value of -2, and find that the second derivative is positive, at the SU(3)-flavor symmetric point on the Columbia plot parametrized with the strange quark mass m_{s} and degenerated up-down quark mass m_{l}.

DOI: 10.1103/PhysRevD.94.114507

I. INTRODUCTION

The Columbia phase diagram plot [1] represents nature of finite temperature phase transition of $2+1$ flavor QCD at zero chemical potential in the plane of the light quark mass and strange quark mass (m_{l}, m_{s}). In the small quark mass region, it is believed that the transition is of first order [2], which turns into a region of crossover as quark masses are increased. The boundary that separates the two regions is the critical endline (CEL), which belongs to the Z_2 universality class [3].

There is a longstanding issue that the results for the critical endpoint (CEP) of 3 flavor QCD at zero chemical potential obtained by Wilson type and staggered type fermion actions are inconsistent [4–10]. Recently, we have investigated CEP with degenerate $N_{\mathrm{f}}=3$ dynamical flavors of nonperturbatively $O(a)$-improved Wilson fermion action, and determined its location by the intersection points of kurtosis for the temporal sizes $N_{\mathrm{T}}=4$, 6 and 8 [11]. The continuum extrapolation implies a nonzero value $m_{\mathrm{PS,CEP}}\approx 300$ MeV for the pseudoscalar meson mass. Scaling violations are large, however, necessitating further studies at larger N_{T} to obtain conclusive results for CEP.

In this article, we explore the properties of CEL. In particular we ask how the CEL curves away from the SU(3)-flavor symmetric point [we denote the SU(3)-flavor symmetric quark mass on the CEL as m^{sym}]. This is a first step to obtain a comprehensive view on the relation of CEL and the physical point for which the strange quark mass is significantly heavier than the degenerate up-down quark mass. To set the stage for our analysis, let us consider the kurtosis $K_{\mathcal{O}}$ of some quantity $\mathcal{O}$ which can be either a gluonic or quark quantity. The kurtosis generally depends on the quark masses m_{u}, m_{d}, and m_{s}, and its Taylor expansion around m^{sym} will have a form $K_{\mathcal{O}}=K_0+(\delta m_{\mathrm{u}}+\delta m_{\mathrm{d}}+\delta m_{\mathrm{s}})K_1+O(\delta m^2)$, where $\delta m_q(q=\mathrm{u},\mathrm{d},\mathrm{s})$ denotes the difference from m^{sym}. Therefore, if one varies the quark masses while keeping the average over the three quark masses, i.e., $\delta m_{\mathrm{u}}+\delta m_{\mathrm{d}}+\delta m_{\mathrm{s}}=0$, the kurtosis remains unchanged up to second order in the variation of the quark masses. For a degenerate up and down quark mass, we have $\delta m_{\mathrm{l}}=\delta m_{\mathrm{u}}=\delta m_{\mathrm{d}}$, and hence the change becomes

$$\delta m_{\mathrm{s}}=-2\delta m_{\mathrm{l}}. \tag{1}$$

This means that the slope of CEL at m^{sym} should take the value -2 on the Columbia plot.

There are no such constraints on the second derivative of CEL with respect to m_{l} at m^{sym}. If it is positive, CEL would smoothly curve up to the tricritical point $m_{\mathrm{s}}=m_{\mathrm{s}}^{\mathrm{tric}}$ located on the axis for the strange quark mass around which CEL is expected to behave as $m_{\mathrm{s}}-m_{\mathrm{s}}^{\mathrm{tric}}\sim m_{\mathrm{l}}^{2/5}$ [12]. So far, a lattice QCD result obtained by using staggered fermions at $N_{\mathrm{T}}=4$ with a lattice spacing $a\approx 0.3$ fm supports such a curve [10]. In this paper, we will also address this issue by using Wilson-type fermions.

This paper is organized as follows. In Sec. II we present the simulation details, including the parameters and the simulation algorithm. Our numerical results are presented in Sec. III. In Sec. IV, we provide a brief conclusion.

*nakamura@riken.jp
†takeda@hep.s.kanazawa-u.ac.jp

II. SIMULATION DETAILS

We perform the kurtosis intersection method [11] to determine CEP and also a multiparameter, multiensemble reweighting method [13] for CEL away from $m^{\rm sym}$. All observables for $N_{\rm f}=2+1$ QCD are computed by using a κ reweighting from $N_{\rm f}=3$ configurations, which were generated in our previous study [11]. We will see that a κ reweighting is very useful to determine many CEPs such as a continuous line around $m^{\rm sym}$ without doing new ensemble generation. This is our motivation to use the reweighting method even in the zero density case. The details of κ reweighting are given in the Appendix. Here we only mention that the evaluation of the determinant in the reweighting factor is approximately done by using the expansion of the logarithm of the determinant to fourth order [14]. The validity of this approximation will be addressed in the next section.

Calculations are made at a temporal lattice size $N_{\rm T}=6$ and the spacial sizes $N_{\rm L}=10$, 12, 16, and 24, with $N_{\rm f}=3$ degenerate flavors of dynamical quarks using the Iwasaki gluon action [15] and the nonperturbatively $O(a)$-improved Wilson fermion action [16]. The periodic boundary condition is imposed for gluon fields while the antiperiodic boundary condition is employed for quark fields. We use a highly optimized HMC code [17], applying mass preconditioning [18] and RHMC [19], the second order minimum norm integration scheme [20]. We put the pseudofermion action on multiple time scales [21] and use a minimum residual chronological method [22] to choose the starting guess for the solver. We generate 63 ensembles of $O(100,000)$ trajectories on HA-PACS and COMA at University of Tsukuba, System E at Kyoto University and PRIMERGY CX400 tatara at Kyushu University. Measurements are done at every 10th trajectory and statistical errors are estimated by the jackknife method with the bin size of $O(1,000)$ configurations. In Table I, we summarize the simulation parameters and statistics.

TABLE I. Simulation parameters and statistics for $N_{\rm f}=3$ runs.

		Number of configurations			
β	κ	$N_{\rm L}=10$	$N_{\rm L}=12$	$N_{\rm L}=16$	$N_{\rm L}=24$
1.715	0.140900	7300	4200		
1.715	0.140920	8000	3800		
1.715	0.140940	8000	8600	7900	
1.715	0.140950	8100	7900	8000	
1.715	0.140960	9500	8800	7900	
1.715	0.140970	9400	6900	8400	
1.715	0.140980	9699	6800	8800	
1.715	0.140990	9500	6300	8599	
1.715	0.141000	10000	8700	9400	
1.715	0.141010	8800	8500	8300	
1.715	0.141020	8700	8900	8600	
1.715	0.141100	8600			
1.73	0.140420	7900	7900	8900	5250
1.73	0.140430	7900	7900	8900	5100
1.73	0.140440	7900	7900	8900	5200
1.73	0.140450	8600	7900	7300	4900
1.75	0.139620	12200	10450	10100	
1.75	0.139640	12900	10400	10100	
1.75	0.139660	11700	10450	10100	
1.75	0.139680	12900	10400	9700	
1.75	0.139700	8378	4900	10100	

As a probe to study the phase structure, we use the quark condensate, which is not a real order parameter at finite quark mass, but will be a real order parameter in the chiral limit. In this study, we use the susceptibility, χ, of the quark condensate to determine the transition point, and its kurtosis, K, for intersection analysis to locate CEL. The quark condensate, Σ, and skewness, S, are used to check that the transition point is determined appropriately. The quantities Σ, χ, S, and K are defined by

$$\begin{aligned}
\Sigma &= \frac{\langle Q_1\rangle}{N_{\rm L}^3 N_{\rm T}},\\
\chi &= \frac{\langle Q_2\rangle - \langle Q_1\rangle^2}{N_{\rm L}^3 N_{\rm T}},\\
S &= \frac{\langle Q_3\rangle - 3\langle Q_2\rangle\langle Q_1\rangle + 2\langle Q_1\rangle^3}{(\langle Q_2\rangle - \langle Q_1\rangle^2)^{3/2}},\\
K &= \frac{\langle Q_4\rangle - 4\langle Q_3\rangle\langle Q_1\rangle - 3\langle Q_2\rangle^2 + 12\langle Q_2\rangle\langle Q_1\rangle^2 - 6\langle Q_1\rangle^4}{(\langle Q_2\rangle - \langle Q_1\rangle^2)^2},
\end{aligned} \tag{2}$$

where the quark loop contributions $Q_{1,2,3,4}$,

$$\begin{aligned}
Q_1 &= N_{\rm f}{\rm tr}[D_f^{-1}],\\
Q_2 &= -N_{\rm f}{\rm tr}[D_f^{-2}] + (N_{\rm f}{\rm tr}[D_f^{-1}])^2,\\
Q_3 &= 2N_{\rm f}{\rm tr}[D_f^{-3}] - 3N_{\rm f}^2{\rm tr}[D_f^{-2}]{\rm tr}[D_f^{-1}] + (N_{\rm f}{\rm tr}[D_f^{-1}])^3,\\
Q_4 &= -6N_{\rm f}{\rm tr}[D_f^{-4}] + 8N_{\rm f}^2{\rm tr}[D_f^{-3}]{\rm tr}[D_f^{-1}] + 3(N_{\rm f}{\rm tr}[D_f^{-2}])^2\\
&\quad - 6N_{\rm f}{\rm tr}[D_f^{-2}](N_{\rm f}{\rm tr}[D_f^{-1}])^2 + (N_{\rm f}{\rm tr}[D_f^{-1}])^4,
\end{aligned} \tag{3}$$

with the Wilson-Clover Dirac operator D_f,

$$\begin{aligned}
D_f &= \frac{1}{2\kappa_f} + \frac{i}{4}c_{\rm sw}\sigma_{\mu\mu}F_{\mu\nu}(n)\delta_{m,n}\\
&\quad - \frac{1}{2}\sum_{\mu=1}^{4}[(1-\gamma_\mu)U_\mu(n)\delta_{n,m+\hat{\mu}}\\
&\quad + (1+\gamma_\mu)U_{-\mu}(n)\delta_{n,m-\hat{\mu}}].
\end{aligned} \tag{4}$$

The trace in Eq. (3) is taken for color, spinor, and coordinate space and numerically estimated by the stochastic method using 20 noises that is checked to be sufficient to control the noise errors. There are some choices for the quark condensate in $N_{\rm f}=2+1$ QCD.

For example, Eq. (2) for $\bar{s}s$ is defined by $\kappa_f = \kappa_s$ and $N_f = 1$. In this study, we choose $\kappa_f = \kappa_l$ and $N_f = 2$ since the signal for $\bar{u}u + \bar{d}d$ and its higher moments turns out to be better than the others. Even if we made different choices, we expect to obtain the same results because all such "order parameters" would behave equally as pure magnetization in the thermodynamic limit.

III. RESULTS

We check first the validity of the reweighting from $N_f = 3$ to $N_f = 2 + 1$. Figure 1 compares Σ, χ, S, and K obtained by the reweighting of the $N_f = 3$ runs at $\beta = 1.73$ with direct $N_f = 2 + 1$ simulations at $(\beta, N_L, \kappa_s) = (1.73, 12, 139500)$ as a function of κ_l. They are in good agreement with each other. Note that in Fig. 1, the multi-ensemble reweighting curve is obtained by using only $N_f = 3$ data without using $N_f = 2 + 1$. Thus, there is no statistical correlation between the curve and direct data points. The statistics for $N_f = 2 + 1$ direct simulations are O(4000–8000) configurations. This is 4–8 times smaller statistics than that used in the reweighting curve. Therefore, the error of the reweighting result is much smaller than that of direct simulations.

The reweighting results for the susceptibility and kurtosis are illustrated in Fig. 2 for $\beta = 1.715$ and 1.73 and three values of κ_s as a function of κ_l. The peak position of susceptibility gives us a very precise value of κ_l for the transition point, and a corresponding value of kurtosis, for each β, κ_s, and N_L. We observe that the volume dependence of the transition point κ_l is mild; thus we extrapolate to the infinite volume limit with a simple $1/N_L^3$ correction term. The resulting transition line in the thermodynamic limit projected on the (β, κ_l) plane is plotted in Fig. 3. Each line corresponds to the interpolated transition line with the functional form for each value of κ_s,

$$\kappa_l = c_0 + c_1\beta + c_2\beta^2. \quad (5)$$

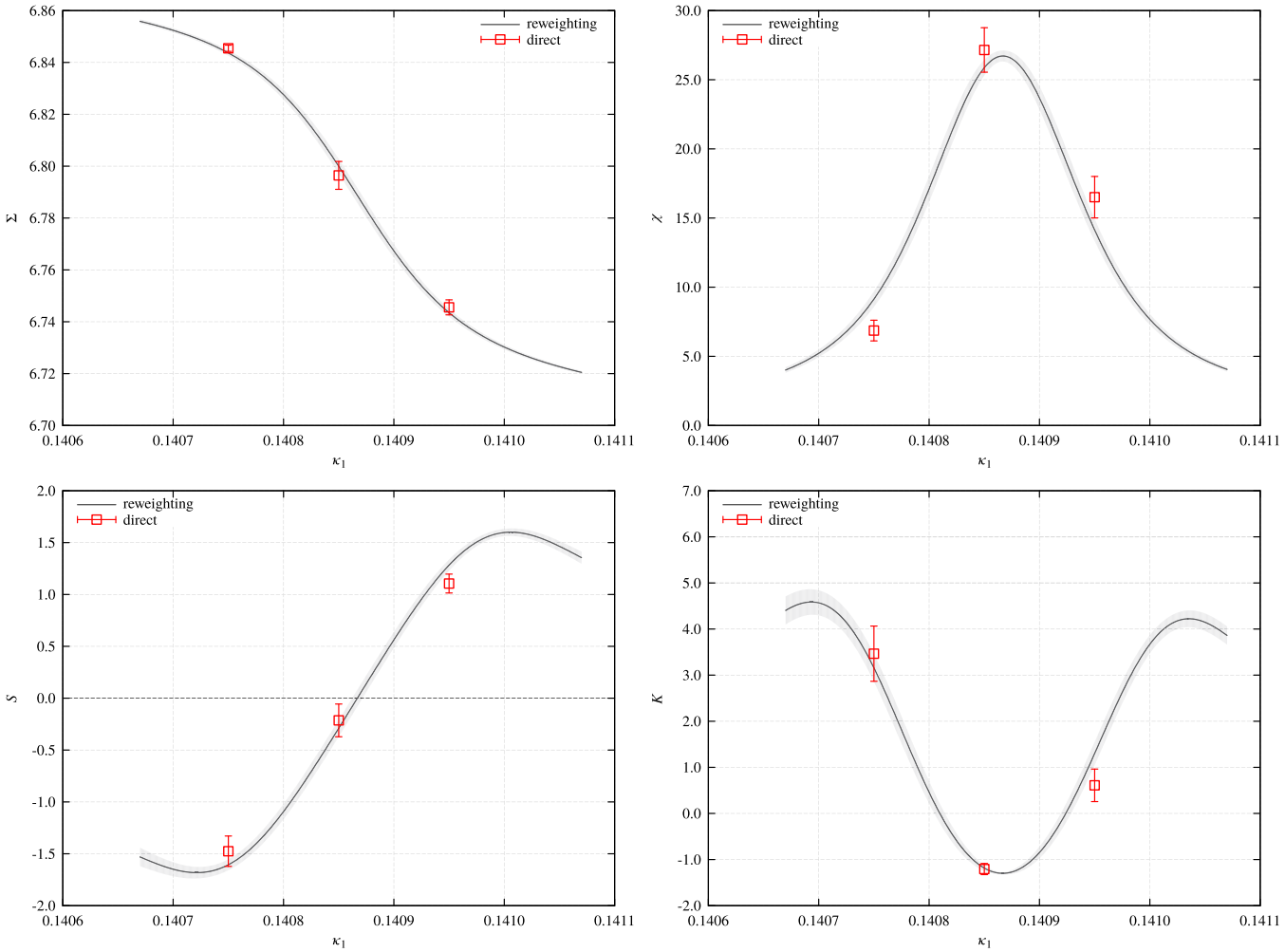

FIG. 1. Σ (top left), χ (top right), S (bottom left), and K (bottom right) as a function of κ_l obtained by the reweighting of $N_f = 3$ data in Table I (curves) and those at $\beta = 1.73$, $\kappa_s = 0.13950$, $N_L = 12$ obtained by the direct $N_f = 2 + 1$ simulations (square data points).

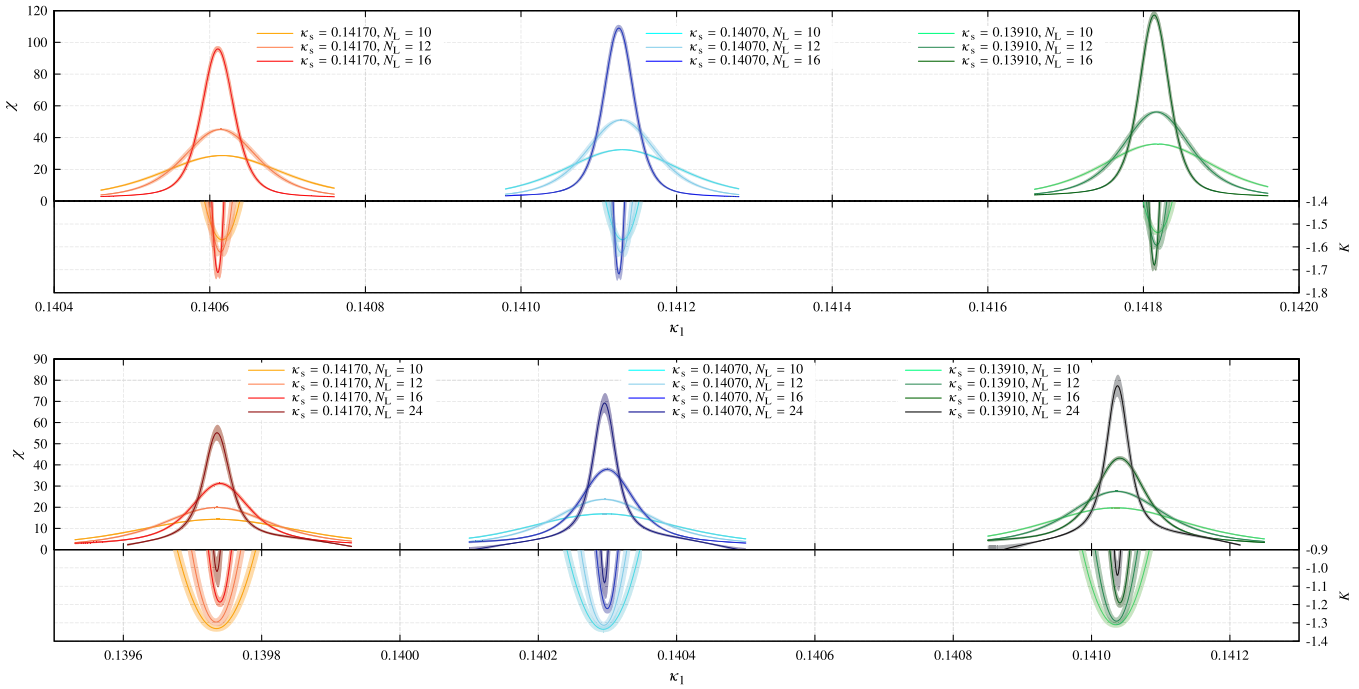

FIG. 2. χ and K for $\kappa_s = 0.13910$, 0.14070, and 0.14170 as a function of κ_l at $\beta = 1.715$ (upper) and 1.73 (lower).

Figure 4 shows the kurtosis at the transition point for three values of κ_s in Fig. 2 as a function of β with various fitting results (dashed lines). The fitting ansatz inspired by a finite-size scaling to second order is given by

$$K = K_E + AN_L^{1/\nu}(\beta - \beta_E) + BN_L^{2/\nu}(\beta - \beta_E)^2, \quad (6)$$

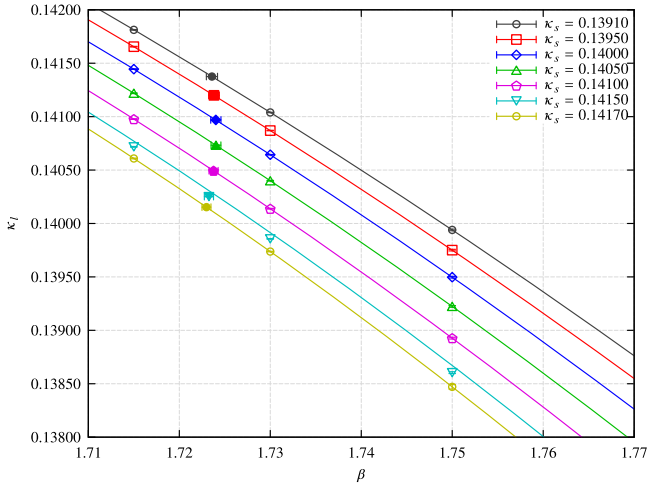

FIG. 3. Phase diagram in bare parameter space of (β, κ_l). Each line represents a transition line with the quadratic form in Eq. (5) for each value of κ_s. Open symbols denote transition points at $\beta = 1.715$, 1.73, and 1.75. Filled symbols denote critical end points. Note that the values of β at critical end points are almost constant for $0.1391 \leq \kappa_s \leq 0.1417$.

where β_E and K_E are the values of β and K at each CEP and ν is the critical exponent along CEL. Here A and B are also fitting parameters. We examine three cases of fitting, namely, (1) the linear functional form [no B-term in Eq. (6)] with two β points, (2) the linear functional form with three β points, and (3) the quadratic functional form Eq. (6) with three β points. The resulting fitting parameters for the three values of κ_s are summarized in Table II. All three cases show consistent results on β_E, K_E, and ν with reasonable χ^2/d.o.f.; thus this kurtosis intersection analysis is shown to be robust. In the end, we decide to use values of fitting parameters obtained by the first choice in the following analysis, and the values of β_E, K_E, and ν in $0.13910 \leq \kappa_s \leq 0.14170$ are summarized in Table III. We find that ν and K_E are consistent with the values of the three-dimensional Z_2 universality class in the range of κ_s. The results for $\kappa_s < 0.13910$ or $\kappa_s > 0.14170$ are too noisy to determine CEP because they are too far away from the original simulation points along the SU(3)-symmetric line. Table III also lists the value of $\kappa_{l,E}$. To obtain this, we go back to the analysis in Fig. 3. Using the interpolated formula of the transition line for a given κ_s, we obtain $\kappa_{l,E}$ by setting $\beta = \beta_E$ as input.

In Fig. 5, we plot $1/\kappa_{s,E}$ as a function of $1/\kappa_{l,E}$ by open circles; they represent our estimate of CEL. The error of β_E in Table III has been propagated to that of $\kappa_{l,E}$. We also plot the points where we have performed zero temperature simulations to calculate the pseudoscalar meson masses. We have generated $O(500)$ configurations at $\beta = 1.72$

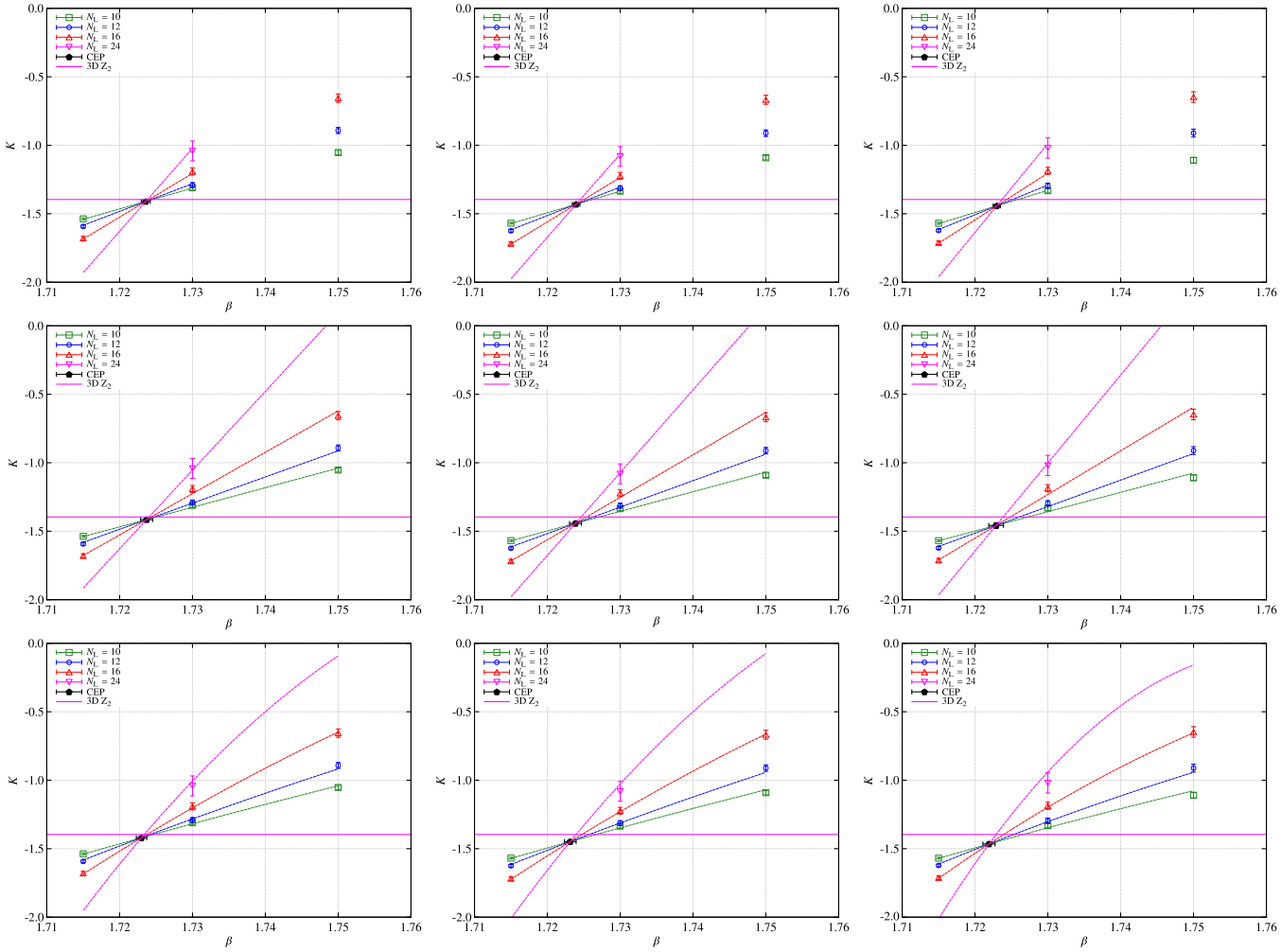

FIG. 4. Typical kurtosis intersection plots for $\kappa_s = 0.13910$, 0.14070, and 0.14170 from left to right, and the linear functional form with two β points (top), linear with three points (middle), and quadratic with three points (bottom).

on a $16^3 \times 32$ lattice for each (κ_l, κ_s). The simulation parameters together with the Wilson flow scale $\sqrt{t_0}/a$ [23] and pseudoscalar meson masses are summarized in Table IV.

To calculate the pseudoscalar meson masses along the CEL, a linear interpolation in Ward identity quark masses is sufficiently good in such a tiny parameter region. Thus, we perform a fit constrained by flavor symmetry of the form

TABLE II. Fit results for Eq. (6) with various choices are summarized. The meaning of fit forms such as "Linear +2 points" is defined in the text.

κ_s	Fit form	β_E	K_E	ν	A	B	χ^2/d.o.f.
0.13910	Linear +2 points	1.72359(61)	−1.410(13)	0.633(46)	0.40(12)	⋯	0.58
0.13910	Linear +3 points	1.72370(82)	−1.415(15)	0.630(39)	0.369(92)	⋯	1.17
0.13910	Quadratic +3 points	1.72300(71)	−1.420(12)	0.607(33)	0.334(73)	−0.0141(77)	0.80
0.14070	Linear +2 points	1.72396(52)	−1.431(11)	0.647(39)	0.45(11)	⋯	0.43
0.14070	Linear +3 points	1.72387(81)	−1.443(16)	0.608(40)	0.325(90)	⋯	1.48
0.14070	Quadratic +3 points	1.72314(80)	−1.448(14)	0.593(37)	0.304(79)	−0.0113(79)	1.19
0.14170	Linear +2 points	1.72299(49)	−1.443(11)	0.631(38)	0.42(10)	⋯	0.47
0.14170	Linear +3 points	1.7229(10)	−1.458(20)	0.578(50)	0.26(10)	⋯	2.35
0.14170	Quadratic +3 points	1.72193(83)	−1.465(15)	0.554(41)	0.234(78)	−0.0096(68)	1.50

TABLE III. Fitting results for the kurtosis intersection whose fitting form is linear in β and includes two β points; namely, $\beta_{\rm E}$, $K_{\rm E}$, and ν for each $\kappa_{\rm s}$ are summarized. On the other hand, $\kappa_{\rm l,E}$ is obtained by interpolation with $\beta_{\rm E}$ as input after fitting with the quadratic function of β in Eq. (5). See text for more details. The error of $\kappa_{\rm l,E}$ contains only that from the interpolation formula but the error of $\beta_{\rm E}$ is not yet propagated to that of $\kappa_{\rm l,E}$ at this point. $\kappa_{\rm s,E}$ have no error because we fix them as target parameters of the reweighting method. The values of $K_{\rm E}$ and ν are roughly consistent with those of the three-dimensional Z_2 universality class, that is, -1.396 and 0.63, respectively.

$\kappa_{\rm s,E}$	$\beta_{\rm E}$	$\kappa_{\rm l,E}$	$K_{\rm E}$	ν
0.13910	1.72359(61)	0.1413751(20)	−1.410(13)	0.633(46)
0.13920	1.72364(60)	0.1413321(21)	−1.411(13)	0.635(46)
0.13930	1.72370(60)	0.1412884(21)	−1.412(13)	0.637(45)
0.13940	1.72376(59)	0.1412441(21)	−1.414(12)	0.638(45)
0.13950	1.72381(58)	0.1411993(20)	−1.415(12)	0.639(44)
0.13960	1.72386(57)	0.1411540(21)	−1.416(12)	0.641(44)
0.13970	1.72391(57)	0.1411085(21)	−1.417(12)	0.642(43)
0.13980	1.72395(56)	0.1410623(21)	−1.418(12)	0.643(43)
0.13990	1.72398(56)	0.1410159(21)	−1.420(12)	0.644(42)
0.14000	1.72401(56)	0.1409692(21)	−1.421(12)	0.645(42)
0.14010	1.72404(55)	0.1409220(21)	−1.422(12)	0.645(42)
0.14020	1.72405(55)	0.1408747(59)	−1.423(12)	0.646(42)
0.14030	1.72406(55)	0.1408273(21)	−1.425(12)	0.646(42)
0.14040	1.72405(54)	0.1407798(22)	−1.426(12)	0.646(41)
0.14050	1.72403(53)	0.1407324(28)	−1.428(12)	0.646(41)
0.14060	1.72400(53)	0.1406849(22)	−1.429(11)	0.647(40)
0.14070	1.72396(52)	0.1406374(22)	−1.431(11)	0.647(39)
0.14080	1.72390(51)	0.1405899(22)	−1.433(11)	0.646(39)
0.14090	1.72384(50)	0.1405421(22)	−1.434(11)	0.646(38)
0.14100	1.72376(49)	0.1404941(27)	−1.436(11)	0.645(38)
0.14110	1.72368(49)	0.1404459(22)	−1.437(11)	0.643(38)
0.14120	1.72359(49)	0.1403976(23)	−1.439(11)	0.641(38)
0.14130	1.72349(49)	0.1403490(22)	−1.440(11)	0.639(38)
0.14140	1.72338(49)	0.1403004(23)	−1.441(11)	0.636(38)
0.14150	1.72326(50)	0.1402515(23)	−1.442(11)	0.633(38)
0.14160	1.72312(50)	0.1402023(27)	−1.443(11)	0.631(38)
0.14170	1.72299(49)	0.1401529(28)	−1.443(11)	0.631(38)

$$
\begin{aligned}
(am_\pi)^2 &= 2A_1\overline{m}_{\rm l} + 2A_2\overline{m}_{\rm s},\\
(am_K)^2 &= (A_1+A_3)\overline{m}_{\rm l} + (A_2+A_4)\overline{m}_{\rm s},\\
(am_{\eta_{\rm s}})^2 &= 2A_3\overline{m}_{\rm l} + 2A_4\overline{m}_{\rm s},\\
\sqrt{t_0}/a &= A_5 + 2A_6\overline{m}_{\rm l} + A_6\overline{m}_{\rm s},
\end{aligned}
\tag{7}
$$

where $\overline{m}_{\rm l} = 1/\kappa_{\rm l} - 1/\kappa_0$ and $\overline{m}_{\rm s} = 1/\kappa_{\rm s} - 1/\kappa_0$. We obtain $\kappa_0 = 0.1419248(25)$, $A_1 = 3.0896(55)$, $A_2 = 0.8494(37)$, $A_3 = 1.8091(54)$, $A_4 = 2.1228(38)$, $A_5 = 0.87742(43)$, $A_6 = -0.5034(20)$, and $\chi^2/\text{d.o.f.} = 16.9$.

Figure 6 shows the results for $(\sqrt{t_0}m_\pi)^2$ and $(\sqrt{t_0}m_{\eta_{\rm s}})^2$ along the CEL. We fit the data points by the following third order polynomial function with the constraint of -2 slope at the symmetric point. The data points are also fitted by

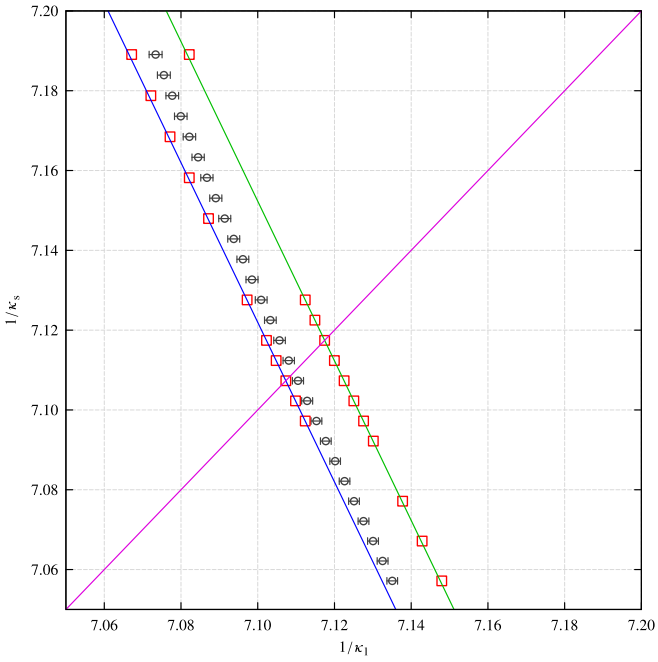

FIG. 5. Results for the critical endpoints in the plane of $1/\kappa_{\rm l}$ and $1/\kappa_{\rm s}$ (black open circles). Also shown (red squares) are the points where zero temperature simulations are carried out to calculate hadron masses. An SU(3)-symmetric line is drawn in pink, while for the green and blue lines the sum of three quark masses is constant.

Eq. (8) with $b_2 = 0$ in order to check higher order contributions against the second derivative.

$$f(x) = b_0 - 2(x-b_0) + b_1(x-b_0)^2 + b_2(x-b_0)^3, \tag{8}$$

where $f(x) = (\sqrt{t_0}m_{\eta_{\rm s}})^2$ and $x = (\sqrt{t_0}m_\pi)^2$. The fit results are given in Table V. We find that the results are reasonably consistent with a slope of -2 and a positive second derivative at CEP.

IV. SUMMARY

We have investigated the CEL of the finite temperature phase transition of QCD with nonperturbatively $O(a)$-improved Wilson-clover fermion action around the SU(3)-symmetric point at zero chemical potential and $N_{\rm T} = 6$. Our method of kurtosis intersection point analysis aided by multiparameter, multiensemble reweighting works well. As a result, we could precisely determine the CEL over a range $0.25 \le (\sqrt{t_0}m_\pi)^2 \le 0.35$, sandwiching the SU(3)-symmetric point at $(\sqrt{t_0}m_\pi)^2 \approx 0.3$, and found -2 for the slope and a positive second derivative around $m^{\rm sym}$ on the Columbia plot.

We need to add to the remarks on our results. First, for zero temperature simulations, we used a slightly different β than $\beta_{\rm E}$. We think that this difference will not change our conclusion since it is only an effect of 0.3% or so in hadron

TABLE IV. $\sqrt{t_0}/a$ and pseudoscalar masses in lattice units at $\beta = 1.72$ on $16^3 \times 32$.

κ_l	κ_s	$\sqrt{t_0}/a$	am_π	am_K	am_{η_s}
0.140600	0.140900	0.78338(31)	0.7054(10)	0.6917(10)	0.6778(10)
0.140650	0.140800	0.78324(33)	0.7015(10)	0.6947(10)	0.6878(10)
0.140700	0.140700	0.78391(32)	0.6960(11)	0.6960(11)	0.6960(11)
0.140750	0.140600	0.78369(31)	0.6925(11)	0.6994(11)	0.7063(11)
0.140800	0.140500	0.78331(31)	0.6881(13)	0.7019(13)	0.7154(13)
0.140900	0.140300	0.78397(43)	0.6755(13)	0.7032(13)	0.7300(13)
0.141100	0.139900	0.78420(39)	0.6573(12)	0.7133(12)	0.7654(12)
0.141200	0.139700	0.78538(33)	0.6444(10)	0.7146(10)	0.7788(09)
0.141300	0.139500	0.78639(25)	0.6319(12)	0.7170(11)	0.7936(11)
0.141400	0.139300	0.78784(27)	0.6174(12)	0.7174(11)	0.8059(10)
0.141500	0.139100	0.78799(45)	0.6018(14)	0.7173(12)	0.8176(11)
0.139900	0.141700	0.77075(28)	0.7996(11)	0.7226(11)	0.6368(12)
0.140000	0.141500	0.77037(26)	0.7895(16)	0.7252(17)	0.6549(18)
0.140100	0.141300	0.77002(25)	0.7835(09)	0.7321(09)	0.6770(10)
0.140250	0.141000	0.76907(26)	0.7722(09)	0.7401(09)	0.7067(09)
0.140300	0.140900	0.76882(27)	0.7696(11)	0.7438(11)	0.7172(11)
0.140350	0.140800	0.76894(27)	0.7652(11)	0.7459(11)	0.7260(11)
0.140400	0.140700	0.76868(27)	0.7620(14)	0.7491(14)	0.7360(14)
0.140450	0.140600	0.76857(27)	0.7583(11)	0.7519(11)	0.7453(11)
0.140500	0.140500	0.76843(27)	0.7542(12)	0.7542(12)	0.7542(12)
0.140550	0.140400	0.76875(27)	0.7491(10)	0.7555(10)	0.7620(10)
0.140600	0.140300	0.76887(28)	0.7428(11)	0.7558(11)	0.7687(11)
0.141200	0.139100	0.77111(26)	0.6845(11)	0.7780(10)	0.8619(10)

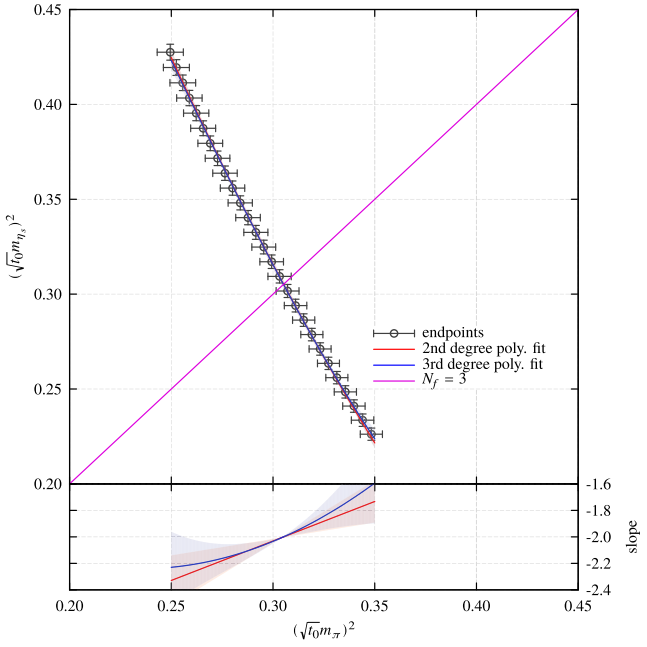

FIG. 6. CEL in the plane of $(\sqrt{t_0}m_\pi)^2$ and $(\sqrt{t_0}m_{\eta_s})^2$ and the slope along CEL calculated by the fit in Eq. (8). The pink line denotes the line of SU(3) symmetry ($N_f = 3$).

mass values. Second, our study is conducted at just a single lattice spacing of $a \approx 0.19$ fm. We are pursuing simulations with a larger N_T to obtain conclusive results, especially for the second derivative. Finally, the physical point at $(\sqrt{t_0}m_\pi)^2 \approx 0.01$ is quite far from the SU(3)-symmetric point. Thus, $N_f = 2 + 1$ simulations are needed to investigate CEL as it approaches the physical point.

TABLE V. Results of polynomial fitting for CEL.

Fitting formula	b_0	b_1	b_2	χ^2/d.o.f.
Eq. (8) with $b_2 = 0$	0.30520(66)	3.0(1.8)	⋯	0.027
Eq. (8)	0.30514(67)	3.4(2.0)	16(31)	0.016

ACKNOWLEDGMENTS

The BQCD code [17] was used in this work. This research used computational resources of HA-PACS and COMA provided by the Interdisciplinary Computational Science Program in the Center for Computational Sciences, University of Tsukuba; System E at Kyoto University through the HPCI System Research project (Project ID: hp140180); and PRIMERGY CX400 tatara at Kyushu University. This work is supported by JSPS KAKENHI Grants No. 23740177 and No. 26800130, FOCUS Establishing Supercomputing Center of Excellence and Kanazawa University SAKIGAKE Project.

APPENDIX: MASS PARAMETER REWEIGHTING

We consider the mass parameter reweighting from $N_f = 3$ to $N_f = 2 + 1$. The multiparameter reweighting for bare

quark mass parameters $m_{\rm l}$ (up-down light quark mass) and $m_{\rm s}$ (strange quark mass) can be done by the formula

$$\langle \mathcal{O}(m_{\rm l}, m_{\rm s})\rangle_{m_{\rm l},m_{\rm s}} = \frac{\left\langle \left(\frac{\det D(m_{\rm l})}{\det D(m)}\right)^2 \left(\frac{\det D(m_{\rm s})}{\det D(m)}\right)^1 \mathcal{O}(m_{\rm l}, m_{\rm s})\right\rangle_m}{\left\langle \left(\frac{\det D(m_{\rm l})}{\det D(m)}\right)^2 \left(\frac{\det D(m_{\rm s})}{\det D(m)}\right)^1 \right\rangle_m}, \tag{A1}$$

where $D(m_f) = D_f$ has been assumed. $m_{\rm l}$ and $m_{\rm s}$ are target mass parameters while m is an actual simulation parameter. The average $\langle \ldots \rangle_{m_{\rm l},m_{\rm s}}$ in the lhs is taken by using the Boltzmann factor, including the $N_{\rm f} = 2 + 1$ quark determinant at parameter $m_{\rm l} \neq m_{\rm s}$, while the average $\langle \ldots \rangle_m$ in the rhs is taken by using the Boltzmann factor, including the degenerate $N_{\rm f} = 3$ quark determinant at mass parameter m. In the above equation, we have explicitly written down the bare parameter dependence on the observable $\mathcal{O}(m_{\rm l}, m_{\rm s})$.

In Eq. (A1), one needs to evaluate the reweighting factor,

$$\left(\frac{\det D(m_{\rm l})}{\det D(m)}\right)^2 \left(\frac{\det D(m_{\rm s})}{\det D(m)}\right)^1. \tag{A2}$$

The ratio of quark determinants requires the high cost of computation if one tries to calculate it directly at many target parameter points. Therefore we adopt a cheaper approximation method, that is, the Taylor expansion of the logarithm of the determinant, which is known to have a better convergence property than the other expansion schemes [14],

$$\ln\left(\frac{\det D(m_{\rm l,s})}{\det D(m)}\right) = \sum_{j=1}^{\infty} \frac{\Delta m_{\rm l,s}^j}{j!} \left(\frac{\partial}{\partial m}\right)^j \ln \det D(m), \tag{A3}$$

with

$$\Delta m_{\rm l,s} = m_{\rm l,s} - m = \frac{1}{2\kappa_{\rm l,s}} - \frac{1}{2\kappa}. \tag{A4}$$

Once some leading coefficients in the expansion are calculated, one can easily evaluate the ratio at many reweighted points up to truncation errors. In our calculation, we evaluate the coefficients up to fourth order and the explicit form of the approximated ratio of the determinant is given by

$$\frac{\det D(m_{\rm l,s})}{\det D(m)} \approx \exp\left[\sum_{j=1}^{4} \frac{(-)^{j+1}\Delta m_{\rm l,s}^j}{j} \mathrm{tr} D^{-j}(m)\right]. \tag{A5}$$

For the same reason as the ratio of the determinant, we use an expansion form for the observable. In the following we restrict ourselves to consider an observable that depends on single mass parameter, $\mathcal{O}(m_{\rm l,s})$. Such an observable can also be expanded:

$$\mathcal{O}(m_{\rm l,s}) = \sum_{j=0}^{\infty} \frac{\Delta m_{\rm l,s}^j}{j!} \left(\frac{\partial}{\partial m}\right)^j \mathcal{O}(m). \tag{A6}$$

For the trace of higher powers of the quark propagator that are included in the higher moments of the quark condensate, we apply the following approximation:

$$\mathrm{tr} D^{-1}(m_{\rm l,s}) \approx \mathrm{tr} D^{-1}(m) + \sum_{j=1}^{3} (-)^j \Delta m_{\rm l,s}^j \mathrm{tr} D^{-(j+1)}(m) \tag{A7}$$

$$\mathrm{tr} D^{-2}(m_{\rm l,s}) \approx \mathrm{tr} D^{-2}(m) + \sum_{j=1}^{2} (-)^j (j+1) \times \Delta m_{\rm l,s}^j \mathrm{tr} D^{-(j+2)}(m), \tag{A8}$$

$$\mathrm{tr} D^{-3}(m_{\rm l,s}) \approx \mathrm{tr} D^{-3}(m) + \sum_{j=1}^{1} (-)^j (j+1)(j+2) \times \Delta m_{\rm l,s}^j \mathrm{tr} D^{-(j+3)}(m), \tag{A9}$$

$$\mathrm{tr} D^{-4}(m_{\rm l,s}) \approx \mathrm{tr} D^{-4}(m). \tag{A10}$$

The validity of this approximation for the moments was confirmed in Ref. [11] and furthermore the direct comparison between the reweighting results and the direct simulation results is done in Fig. 1, and then it turns out that the truncation error of this approximation is smaller than the statistical errors in our parameter region.

[1] F. R. Brown, F. P. Butler, H. Chen, N. H. Christ, Z. Dong, W. Schaffer, L. I. Unger, and A. Vaccarino, Phys. Rev. Lett. **65**, 2491 (1990).
[2] R. D. Pisarski and F. Wilczek, Phys. Rev. D **29**, 338 (1984).
[3] S. Gavin, A. Gocksch, and R. D. Pisarski, Phys. Rev. D **49**, R3079 (1994).
[4] S. Aoki *et al.* (JLQCD Collaboration), Nucl. Phys. B, Proc. Suppl. **73**, 459 (1999).

[5] F. Karsch, E. Laermann, and C. Schmidt, Phys. Lett. B **520**, 41 (2001).
[6] D. Smith and C. Schmidt, *Proc. Sci.*, Lattice2011 (2011) 216 [arXiv:1109.6729].
[7] G. Endrődi *et al.*, *Proc. Sci.*, Lattice2007 (2007) 182 [arXiv:0710.0998].
[8] H.-T. Ding *et al.*, *Proc. Sci.*, Lattice2011 (2011) 191 [arXiv:1111.0185].
[9] Y. Iwasaki, K. Kanaya, S. Kaya, S. Sakai, and T. Yoshié, Phys. Rev. D **54**, 7010 (1996).
[10] P. de Forcrand and O. Philipsen, J. High Energy Phys. 01 (2007) 077.
[11] X.-Y. Jin, Y. Kuramashi, Y. Nakamura, S. Takeda, and A. Ukawa, Phys. Rev. D **91**, 014508 (2015).
[12] K. Rajagopal, in *Quark-Gluon Plasma 2*, edited by R. Hwa (World Scientific, Singapore, 1995).
[13] X.-Y. Jin, Y. Kuramashi, Y. Nakamura, S. Takeda, and A. Ukawa, Phys. Rev. D **92**, 114511 (2015).
[14] X. Y. Jin, Y. Kuramashi, Y. Nakamura, S. Takeda, and A. Ukawa, Phys. Rev. D **88**, 094508 (2013).
[15] Y. Iwasaki, Report No. UTHEP-118, 1983.
[16] S. Aoki *et al.* (*CP*-PACS and JLQCD Collaborations), Phys. Rev. D **73**, 034501 (2006).
[17] Y. Nakamura and H. Stüben, *Proc. Sci.*, Lattice2010 (2010) 040 [arXiv:1011.0199].
[18] M. Hasenbusch, Phys. Lett. B **519**, 177 (2001); M. Hasenbusch and K. Jansen, Nucl. Phys. **B659**, 299 (2003).
[19] M. A. Clark and A. D. Kennedy, Phys. Rev. Lett. **98**, 051601 (2007).
[20] I. P. Omelyan, I. M. Mryglod, and R. Folk, Phys. Rev. E **65**, 056706 (2002); Comput. Phys. Commun. **151**, 272 (2003).
[21] J. C. Sexton and D. H. Weingarten, Nucl. Phys. **B380**, 665 (1992).
[22] R. Brower, T. Ivanenko, A. Levi, and K. Orginos, Nucl. Phys. **B484**, 353 (1997).
[23] M. Lüscher, J. High Energy Phys. 08 (2010) 071.